

Article

Synthesis, Structures, and Water Adsorption of Two Coordination Polymers Constructed by M(II) (M = Ni (1) and Zn (2)) with 1,3-Bis(4-Pyridyl)Propane (bpp) and 1,2,4,5-Benzenetetracarboxylate (BT⁴⁻) Ligands

Chih-Chieh Wang ^{1,*}, Wei-Cheng Yi ¹, Zi-Ling Huang ¹, Tsai-Wen Chang ¹, Wen-Chi Chien ¹, Yueh-Yi Tseng ¹, Bo-Hao Chen ², Yu-Chun Chuang ^{2,*} and Gene-Hsiang Lee ³

¹ Department of Chemistry, Soochow University, Taipei 11102, Taiwan; 06333004@gm.scu.edu.tw (W.-C.Y.); wendyhung51@gmail.com (Z.-L.H.); meadow8692@gmail.com (T.-W.C.); momo2013124@gmail.com (W.-C.C.); lunar24575559@gmail.com (Y.-Y.T.)

² National Synchrotron Radiation Research Center, Hsinchu 30076, Taiwan; chen.bh@nsrrc.org.tw

³ Instrumentation Center, National Taiwan University, Taipei 10617, Taiwan; ghlee@ntu.edu.tw

* Correspondence: ccwang@scu.edu.tw (C.-C.W.); chuang.yc@nsrrc.org.tw (Y.-C.C.); Tel.: +886-2-28819471 (ext. 6828) (C.-C.W.)

Received: 31 August 2020; Accepted: 25 September 2020; Published: 27 September 2020



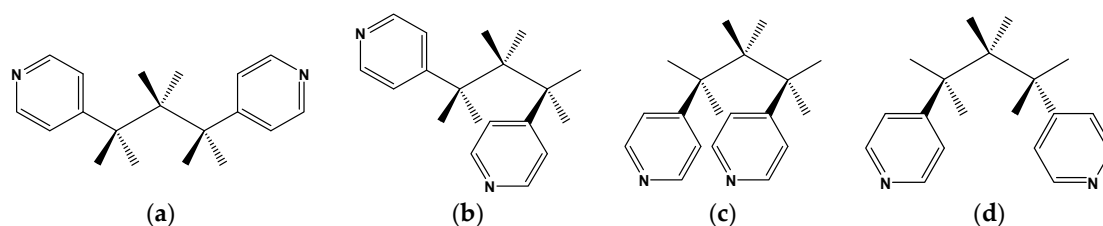
Abstract: Two coordination polymers (CPs), with chemical formulas $[\text{Ni}_2(\text{bpp})_2(\text{BT})(\text{H}_2\text{O})_6] \cdot 1.5(\text{EtOH}) \cdot 1.5\text{H}_2\text{O}]_n$ (**1**) and $[\text{Zn}(\text{bpp})(\text{BT})_{0.5}] \cdot 5\text{H}_2\text{O}$ (**2**) (bpp = 1,3-bis(4-pyridyl)propane, and BT⁴⁻ = tetraanion of 1,2,4,5-benzenetetracarboxylic acid), have been synthesized and structurally characterized by single-crystal X-ray diffraction methods. In compound **1**, the coordination environments of two crystallographically independent Ni(II) ions are both distorted octahedral bonded to two nitrogen donors from two bpp ligands and four oxygen donors from one BT⁴⁻ ligand and three water molecules. Both bpp and BT⁴⁻ act as bridging ligands with *bis*-monodentate and 1,4-*bis*-monodentate coordination modes, respectively, connecting the Ni(II) ions to form a 2D layered metal-organic framework (MOF). Adjacent 2D layers are then arranged orderly in an ABAB manner to complete their 3D supramolecular architecture. In **2**, the coordination environment of Zn(II) ion is distorted tetrahedral bonded to two nitrogen donors from two bpp ligands and two oxygen donors from two BT⁴⁻ ligands. Both bpp and BT⁴⁻ act as bridging ligands with *bis*-monodentate and 1,2,4,5-*tetrakis*-monodentate coordination modes, respectively, connecting the Zn(II) ions to form a 3D MOF. The reversible water de-/adsorption behavior of **1** between dehydrated and rehydrated forms has been verified by cyclic Thermogravimetric (TG) analyses through de-/rehydration processes. Compound **1** also exhibits significant water vapor hysteresis isotherms.

Keywords: coordination polymer; metal-organic framework; hydrogen bonds; water adsorption

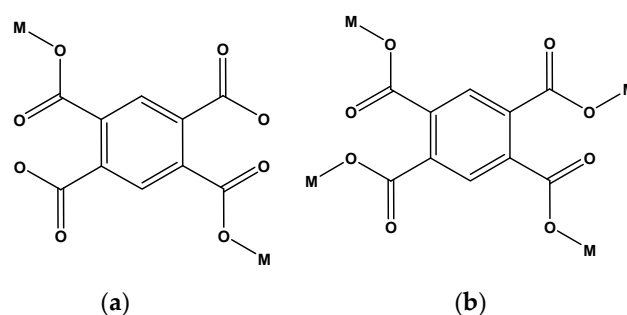
1. Introduction

Coordination compounds with open two-dimensional (2D) or three-dimensional (3D) polymeric metal-organic frameworks (MOFs) [1,2] containing guest solvent molecules are attractive research fields, owing not only to their designable structure with unusual flexibilities but also to their tunable functional application [3–8], which provide the possibility for developing advanced functional materials for assemblies of guest molecules in confined spaces [9,10]. In particular, 1,2,4,5-benzenetetracarboxylic acid (H₄BT) and its de-protonated form of BT⁴⁻ appear attractive as building blocks with template capacity for the construction of 1D, 2D and 3D extended coordination polymers (CPs) [11–27]. In the relevant approach, BT⁴⁻, which possesses a rigid aromatic multi-carboxylate structure, has been used

as a poly-functional ligand, including as a bridging ligand with various coordination modes to build up many CPs or MOFs with novel extended networks and also as a hydrogen bonding acceptor in the stabilization of extended 3D supramolecular networks [11–29]. The combination of BT^{4-} and additional rigid or flexible N-based co-ligands in such synthetic systems can generate interesting polymeric frameworks with different structural topologies [19–21,30–36]. In this regard, bi-pyridyl-type ligand, 1,3-bis(4-pyridyl)propane (bpp), is a flexible bifunctional ligand [31] that can adopt different conformations (TT, TG, GG, GG'; T = trans and G = gauche, as shown in Scheme 1) via the rotation of aliphatic chain $[-\text{CH}_2-\text{CH}_2-\text{CH}_2-]$ between two pyridyl rings to obtain different structural topologies in polymeric structures [34]. Several crystal structures containing transition metal ions and bpp ligands show the formation of 1D, 2D and 3D networks [30–36]. However, the polymeric structures constructed by transition metal ions with BT^{4-} and bpp ligands are rare and only a few polymeric networks have been reported in the literature [19–21]. Focusing on this approach, we report here the synthesis and structural characterization of two CPs, $\{[\text{Ni}_2(\text{bpp})_2(\text{BT})(\text{H}_2\text{O})_6] \cdot 1.5(\text{EtOH}) \cdot 1.5\text{H}_2\text{O}\}_n$ (**1**) and $[\text{Zn}(\text{bpp})(\text{BT})_{0.5}] \cdot 5\text{H}_2\text{O}$ (**2**), in which the BT^{4-} ligands act as the bridging ligands with two kinds of coordination modes, 1,4-*bis*-monodentate in **1** and 1,2,4,5-tetrakis-monodentate in **2** (shown in Scheme 2), and the bpp acts as a bridging ligand with *bis*-monodentate coordination mode, connecting the M(II) ions to generate 2D layered and 3D MOFs, respectively. The thermal stability, reversible de-/adsorption of the guest water molecules and water vapor ad-/desorption isotherms are the focus of this study.



Scheme 1. Possible conformations of 1,3-bis(4-pyridyl)propane (a) TT, (b) TG, (c) GG, (d) GG'; T = trans and G = gauche.



Scheme 2. Coordination modes of (a) 1,4-*bis*-monodentate, (b) 1,2,4,5-tetrakis-monodentate of BT^{4-} ligand used in **1** and **2**, respectively.

2. Experimental Details

2.1. General Procedures

All chemicals were used as commercially obtained. Elemental analyses were conducted with a Perkin-Elmer 2400 elemental analyzer. IR spectra (KBr disk) were recorded on a Nicolet FT IR, MAGNA-IR 500 spectrometer. Thermogravimetric analysis (TGA) was performed on a Perkin-Elmer 7 Series/UNIX TGA7 analyzer. Single-phased powder samples were loaded into alumina pans and heated with a ramp rate of $5\text{ }^\circ\text{C}/\text{min}$ from room temperature to $700\text{ }^\circ\text{C}$ under a nitrogen atmosphere. The water vapor adsorption isotherm at 298 K was measured in the gaseous state by using BELSORP-max volumetric adsorption equipment from BEL, Osaka, Japan. The adsorbent sample ($\sim 100\text{--}150\text{ mg}$),

which was prepared at 150 °C and 10^{-2} Pa for around 24 h, was placed into the sample cell, and then the change in pressure was monitored and the degree of adsorption was determined by the decrease in pressure at equilibrium state.

2.2. Synthesis of $\{[Ni_2(bpp)_2(BT)(H_2O)_6] 1.5(EtOH) 1.5H_2O\}_n$ (**1**)

An ethanol/H₂O solution (1:1, 3 mL) of 1,2,4,5-benzene-tetracarboxylic acid (H₄BT) (0.02 mmol) was added to an ethanol/water (1:1, 6 mL) solution of NiCl₂ (0.04 mmol) and 1,3-bis(4-pyridyl)propane (0.04 mmol) at RT. After standing for one week, blue block crystals of **1** (yield, 53.53%) were obtained. The resulting crystals were filtrated and then washed several times with distilled water. Anal. calc. for (**1**), C₃₉H₅₄N₄O₁₇Ni₂: C 48.37, N 5.78, H 5.58; found: C 48.91, N 5.77, H 5.69. IR: $\nu = 3417$ (vs, br), 1620 (vs), 1571 (vs), 1433 (s), 1414 (s), 1375 (vs), 1324 (m), 1222 (m), 1137 (w), 1072 (m), 1031 (s), 823 (s), 620 (m), 518 (m) cm⁻¹.

2.3. Synthesis of $[Zn(bpp)(BT)_{0.5}] \cdot 5H_2O$ (**2**)

An ethanol/H₂O solution (1:1, 3 mL) of 1,2,4,5-benzene-tetracarboxylic acid (H₄BT) (0.0050g, 0.02 mmol) was added to an ethanol/water (1:1, 6 mL) solution of ZnF₂ (0.0041g, 0.04 mmol) and 1,3-bis(4-pyridyl)propane (0.0079 g, 0.04 mmol) at RT. After standing for several days, colorless needle-like crystals of **2** (yield, 55.8%) were obtained. The resulting crystals were filtrated and then washed several times with distilled water. Anal. calc. for (**2**), C₁₈H₂₅N₂O₉Zn: C 45.15, N 5.84, H 5.22; found: C 45.14, N 5.85, H 5.34. IR: $\nu = 3358$ (vs, br), 1620 (s), 1571 (s), 1484 (m), 1431 (s), 1378 (vs), 1332 (m), 1226 (w), 1137 (w), 1071 (w), 922 (w), 839 (m), 805 (m), 683 (m), 666 (m), 585 (m), 531 (m) cm⁻¹.

2.4. X-ray Crystallography and Refinements

The diffraction data for compounds **1** and **2** were collected on a Siemens SMART diffractometer with Mo radiation ($\lambda = 0.71073$ Å) at 150 K. Cell parameters were retrieved using SMART [37] software and refined with SAINT [38] on all observed reflections. Data reduction was performed with the SAINT [39] software and corrected for Lorentz and polarization effects. Absorption corrections were applied with the program SADABS [39]. Direct phase determination and subsequent difference Fourier map synthesis yielded the positions of all atoms. The final full-matrix, least-squares refinement on F^2 was applied for all observed reflections [$I > 2\sigma(I)$]. All calculations were performed by using the SHELXTL-PC V 5.03 software package [40]. Crystal data and details of the data collection and structure refinements for **1** and **2** are summarized in Table 1. CCDC-2022795 and 2,022,797 for **1** and **2**, respectively, contain the supplementary crystallographic data for this paper (Figures S1 and S2). These data can be obtained free of charge from www.ccdc.cam.ac.uk/conts/retrieving.html or from the Cambridge Crystallographic Data Centre, 12, Union Road, Cambridge CB2 1EZ, UK; fax: (internat.) +44-1223/336-033; email: deposit@ccdc.cam.ac.uk.

Table 1. Crystal data and refinement details of compounds **1** and **2**.

	1	2
empirical formula	C ₃₉ H ₅₄ N ₄ Ni ₂ O ₁₇	C ₁₈ H ₂₅ N ₂ O ₉ Zn
formula mass (g mol ⁻¹)	968.28	478.77
crystal system	Monoclinic	Monoclinic
space group	Cc	P 2 ₁ /c
<i>a</i> (Å)	9.9430(4)	10.5868(5)
<i>b</i> (Å)	19.3122(7)	16.5965(7)
<i>c</i> (Å)	23.3965(8)	12.3099(5)
α (deg)	90	90
β (deg)	98.8698(12)	109.2795(13)
γ (deg)	90	90
<i>V</i> (Å ³)	4438.9(3)	2041.60(15)
<i>Z</i>	4	4

Table 1. Cont.

	1	2
T (K)	150(2)	150(2)
D_{calcd} (g cm^{-3})	1.449	1.558
μ (mm^{-1})	0.924	1.257
θ range (deg)	2.29–27.52	2.38–27.48
total no. of collected data	16656	17257
no. of unique data	9380	4684
no. of obsd data ($I > 2\sigma(I)$)	8689	4329
R_{int}	0.0181	0.0158
refine params	570	311
R_1, wR_2^1 ($I > 2\sigma(I)$)	0.0359, 0.0948	0.0217, 0.0550
R_1, wR_2^1 (all data)	0.0410, 0.0978	0.0247, 0.0564
GOF ²	1.042	1.054

$$^1 R_1 = \sum \|F_o - F_c\| / \sum |F_o|; wR_2(F^2) = [\sum w|F_o^2 - F_c^2|^2 / \sum w(F_o^4)]^{1/2}. ^2 \text{GOF} = \{\sum [w|F_o^2 - F_c^2|^2] / (n - p)\}^{1/2}.$$

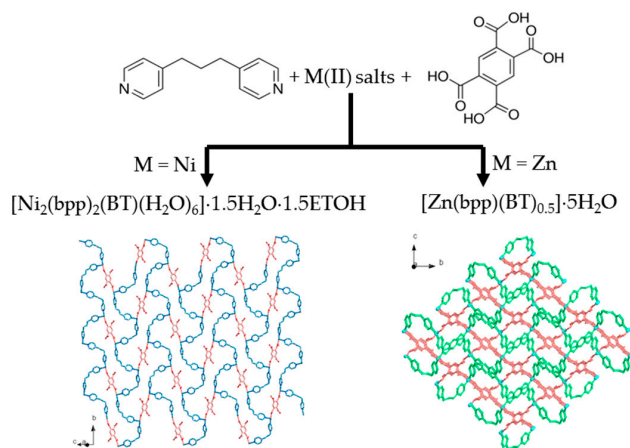
2.5. In Situ X-ray Powder Diffraction

The powder X-ray diffraction measurement of compounds **1** and **2** was performed at the BL01C2 beamline of the National Synchrotron Radiation Research Center (NSRRC) in Taiwan. The X-ray energy was selected at 1.0332 Å. The diffraction pattern was recorded with a Mar345 imaging-plate detector and typical exposure duration of 2 min. The one-dimensional powder diffraction profile was converted with GSAS-II program [41]. The diffraction angles were calibrated according to Bragg positions of lanthanum boride (SRM660b) standards.

3. Results and Discussion

3.1. Synthesis and IR Spectroscopy

Compounds **1** and **2** were synthesized by direct mixing of M(II) salts, bpp and H₄BT with a molar ratio of 2:2:1 to obtain blue rod-like crystals of **1** and colorless needle-like crystals of **2**, respectively. The synthetic representation is shown in Scheme 3. The most relevant IR features are those associated with the BT⁴⁻ and bpp ligands [19,20]. Absorption bands in the range of 1400–1700 cm⁻¹ can be related to the carboxylate groups of BT⁴⁻ ligand and bpp ligand, since the main vibrational frequencies of the two ligands appear in the same spectral region. However, a strong band centered at around 1571 cm⁻¹ in the spectrum can be attributed to vibrational modes representing the C–C and C–N mixing stretching motions and is in agreement with the characteristics of the bpp ligand. Additional broad bands appear in the range of 3100–3500 cm⁻¹ in **1** and **2**, indicating the presence of the O–H stretching vibration from water molecules.

Scheme 3. Synthetic representation of **1** and **2**.

3.2. Structural Characterization of $\{[Ni_2(bpp)_2(BT)(H_2O)_6] \cdot 1.5(EtOH) \cdot 1.5H_2O\}_n$ (**1**)

Compound **1** is iso-structural with that of $\{[Co_2(bpp)_2(BT)(H_2O)_6] \cdot 2H_2O\}_n$ [20] and crystallizes in the monoclinic Cc space group, in which the asymmetric unit is composed of two Ni(II) centers, two bpp, one BT^{4-} ligand, six coordinated H_2O molecules and one and a half solvated H_2O and C_2H_5OH molecules. The molecular structures of **1** are shown in Figure 1a, in which two crystallographically independent Ni(II) ions are both six coordinate bonded to four oxygen donors of one BT^{4-} ligand and three H_2O molecules and two nitrogen donors of two bpp ligands located at the *cis* position, forming a distorted octahedral geometry. Bond lengths and angles around the Ni(II) ions are listed in Table S1 (included in the Supporting Information). In **1**, two crystallographically independent bpp ligands, adopting TT and TG conformations, respectively, both act as bridging ligands with *bis*-monodentate coordination mode connecting the Ni(II) ions to form one-dimensional (1D) zigzag chains (Figure 1b). Adjacent chains are inter-linked via the connectivity between Ni(II) ions and BT^{4-} ligands with 1,4-*bis*-monodentate coordination mode [20] to generate a 2D layered MOF (Figure 1b). The Ni(II)⋯Ni(II) separations via TT-, TG-bpp and BT^{4-} bridges are 12.922(3), 12.203(3) and 11.220(1) Å, respectively. Adjacent 2D layers are then arranged orderly in an ABAB parallel manner to build up their 3D supramolecular architectures (Figure 1c). It is important to note that intra- and inter-layer O–H⋯O hydrogen bonding interactions between the coordinated H_2O molecules and uncoordinated oxygen atoms of BT^{4-} ligands, with O⋯O distances in the range of 2.675(1)–3.170(2) Å, provide extra stabilization energies for the construction of its 3D structures. Furthermore, guest solvent molecules, 1.5 EtOH and 1.5 H_2O , which are located at the vacant spaces in the 3D supramolecular architecture, are reinforced by intermolecular hydrogen bonding interactions between O–H groups of guest molecules and oxygen atoms of coordinated H_2O molecules and BT^{4-} ligands. Relevant parameters of hydrogen bonds are summarized in Table S2 (included in the Supporting Information).

The thermal stability and temperature-dependent structural variation for **1** were studied by thermogravimetric (TG) analysis and in situ powder X-ray diffraction (PXRD) measurements, respectively. During the heating process, the TG analysis of **1** displayed a two-step weight loss (Figure 2a), while the first weight loss of 20.3% corresponded to the weight losses of six coordinated water molecules, 1.5 guest ethanol and 1.5 water molecules (calc. 21.1%), occurring in the range of approximately 33.9–156.9 °C and then remaining thermally stable up to 198.4 without any weight loss. On further heating, these samples decomposed. It is important to note that, during the heating processes, crystals in **1** were accompanied by morphological changes. The simultaneous and gradual color changes of the crystals were followed by optical microscopy, as shown in Figure 2a, during the de-solvation processes at some specific temperatures. A well-formed blue crystal of **1** was obtained. As the temperature was raised, the colors of dried crystals gradually turned from blue to pale-blue, and many chips with random cracks on the crystal surface were observed. In order to gain more structural information, in situ temperature-dependent synchrotron PXRD patterns of **1** were collected from 25 °C to 410 °C, and the results at some specific temperatures are shown in Figure 2b. The PXRD patterns of as-synthesized samples **1** at RT matched well with the simulated one based on the single crystal structures. As the temperature increased, solvent de-solvation processes were initialized at 100 °C for **1** and converted to a meta-stable phase before entire structure collapse. However, due to the poor long-range ordering of PXRD data, the unit cells of dehydrated form **1** could not be determined directly by using synchrotron PXRD data. The temperature-dependent PXRD results are consistent with the TGA results and morphological changes.

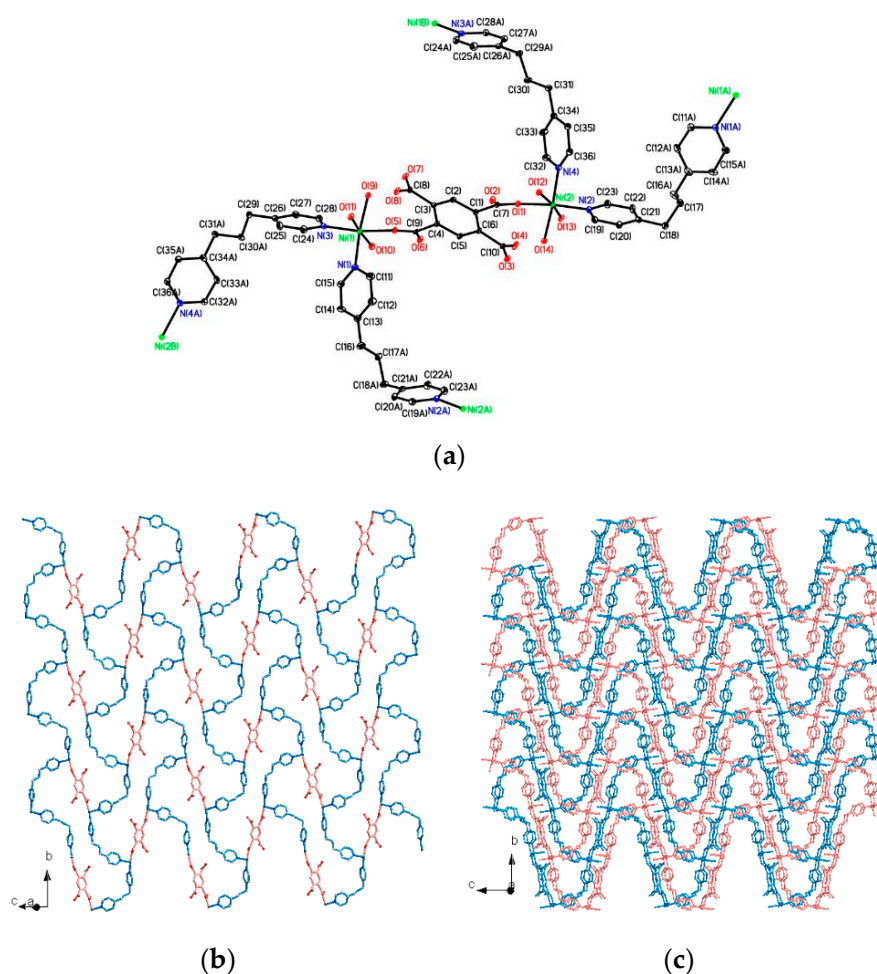


Figure 1. (a) Coordination environments of two Ni(II) ions with atom labeling scheme (ORTEP drawing, 30% thermal ellipsoids). The solvents, ethanol and water molecules and H atoms are omitted for clarity. (b) A 2D layered metal-organic framework (MOF) constructed by bpp (blue) and BT⁴⁻ (red) bridges. Coordinated water molecules and guest ethanol and water molecules are omitted for clarity. (c) The 3D supramolecular architecture. The solvents, ethanol and water molecules and H atoms are omitted for clarity.

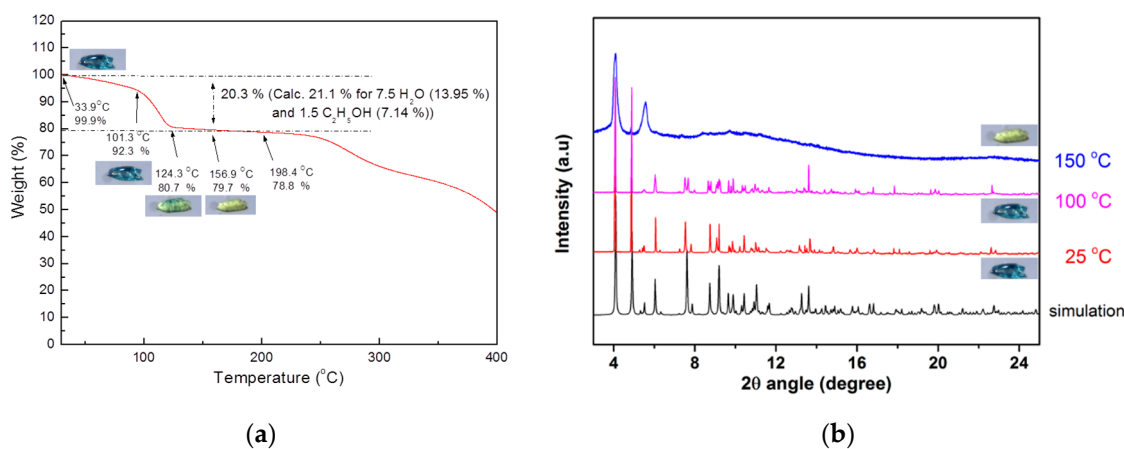


Figure 2. (a) Thermogravimetric (TG) measurement associated with morphological changes at selected temperatures of **1**. (b) Powder X-ray diffraction patterns of **1** at RT and selected temperatures and its simulation from single-crystal diffraction data associated with morphological changes at selected temperatures of **1**. The baselines for each temperature were shifted for clarity.

3.3. Structural Description of $\{[Zn(bpp)(BT)_{0.5}] \cdot 5H_2O\}_n$ (**2**)

Compound **2** crystallizes in the monoclinic $P 2_1/c$ space group, in which the asymmetric unit is composed of one Zn(II) ion, one bpp, half of a BT^{4-} ligand and five guest water molecules. The coordination geometry of Zn(II) ion in **2** is distorted tetrahedral (Figure 3a) bonded to two oxygen donors from two BT^{4-} ligands and two nitrogen donors from two bpp ligands. Relevant bond lengths and angles around the Zn(II) ion are listed in Table S3 (included in the Supporting Information). In **2**, BT^{4-} acts as a bridging ligand with 1,2,4,5-*tetrakis*-monodentate coordination mode [28,29] connecting the Zn(II) ions to form a 2D sinusoidal-like $[Zn_2(BT)]_n$ layered framework (Figure 3b). Adjacent layers are inter-linked via the connectivity between Zn(II) ions and bpp ligands with *bis*-monodentate coordination mode to complete its 3D MOF (Figure 3c), in which five guest water molecules are located at the vacant sites (Figure 3d, right). The Zn(II)⋯Zn(II) separation via the TG-bpp bridge is 10.681(1) Å and via BT^{4-} bridges is 6.170(1), 9.208(1), 11.111(3), 11.057(2) Å (Figure 3c, right), respectively. It is noteworthy that five guest water molecules are assembled together to generate a 2D sinusoidal-like hydrogen-bonded water layer (Figure 3d, left and middle), which is built up by two water cluster units—one is a $(H_2O)_6$ chair-like water ring and the other is a $(H_2O)_{18}$ water ring (Figure 3d, left)—via the intermolecular O–H⋯O hydrogen bonding interactions with the O⋯O distances in the range of 2.725(1)–2.818(1) Å. Importantly, synergistic O–H⋯O hydrogen bonding interactions between guest H_2O molecules in the 2D water layer and carboxylate groups of BT^{4-} ligands in two $[Zn_2(BT)]_n$ layers (Figure 3d, right) provide significant stabilization energy to maintain the accumulation of 2D water layers in the 3D MOF. Relevant parameters for hydrogen bonds are summarized in Table S4 (included in Supporting Information).

During the heating process, the TG analysis (see Figure 4a) revealed that **2** underwent a two-step weight loss, while the first weight loss of 18.1% corresponded to the loss of five guest H_2O molecules (calc. 18.8%), occurring in the range of approximately 30.6–64.3 °C, and then remaining thermally stable up to 291.7 °C without any weight loss. On further heating, the sample decomposed. It is important to note that, during the heating processes, crystal **2** was accompanied by morphological changes. The simultaneous and gradual changes of the crystals were followed by optical microscopy, as shown in Figure 4a, during the dehydration process at some specific temperatures. A well-formed colorless crystal of **2** was obtained. As the temperature was raised, the color of the crystals gradually turned from colorless to white and many chaps with random cracks on the crystal surface were observed. To gain more information on the temperature-dependent structural variation, in situ synchrotron PXRD patterns of **2** were collected from 25 °C to 410 °C, and the results at some specific temperatures are shown in Figure 4b. The PXRD patterns of as-synthesized sample **2** matched well with the simulated pattern based on the single crystal structure. As the temperature increased, a new phase was transformed at 110 °C and could be sustained up to 320 °C. According to the cell refinement results, the cell volume reduced from 2078.88 Å³ to 1847.39 Å³, roughly a 12% reduction. The symmetry was kept in monoclinic lattice, and corresponding cell parameters of hydrated and dehydrated forms were $a = 12.5099$ Å, $b = 14.7892$ Å, $c = 10.8858$ Å, $\beta = 113.469^\circ$ and $a = 10.6860$ Å, $b = 16.5976$ Å, $c = 12.4611$ Å, $\beta = 109.845^\circ$, respectively. The temperature-dependent PXRD results are consistent with the TGA results and morphological changes.

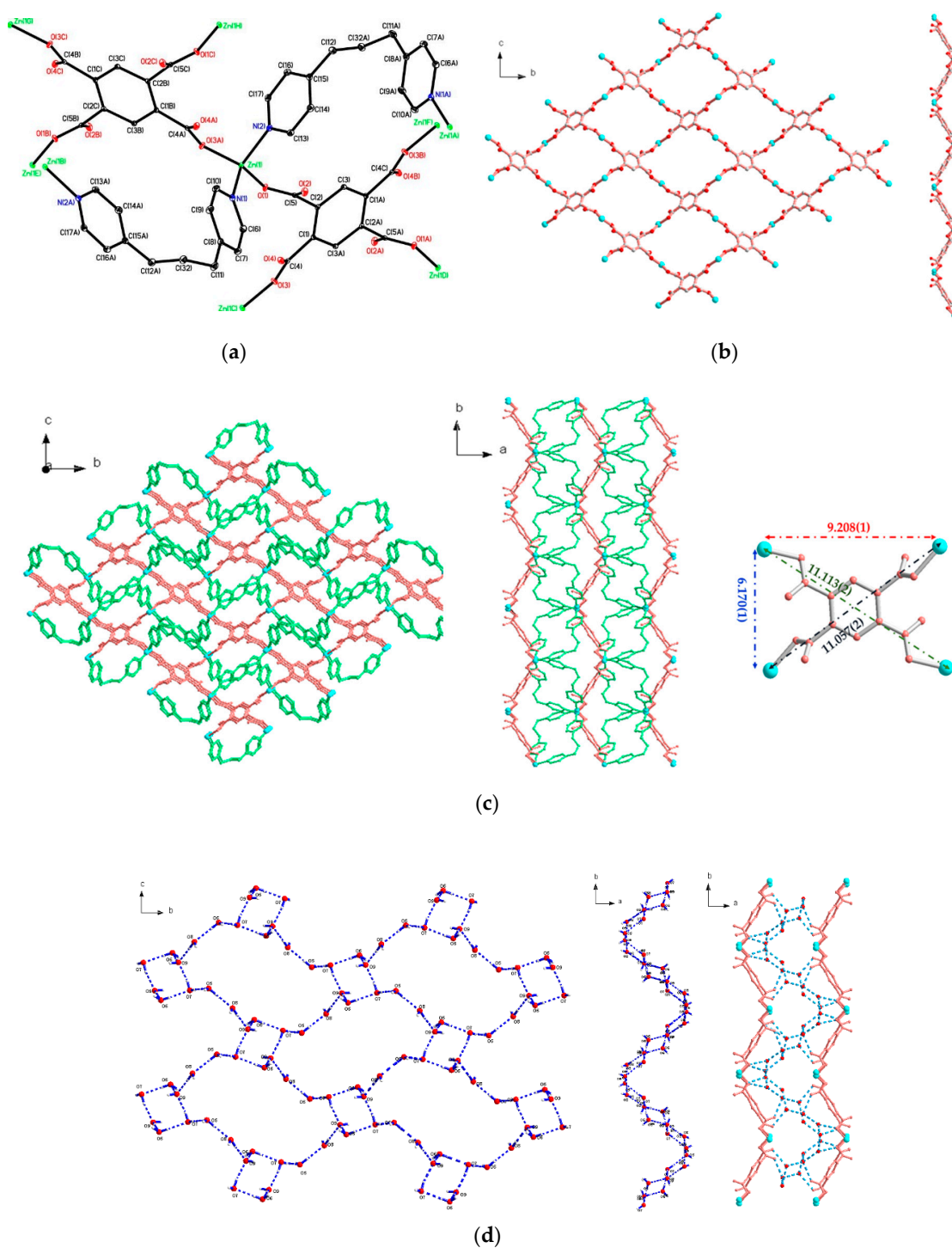


Figure 3. (a) Distorted tetrahedral geometry of Zn(II) ion in **2** with atom labeling scheme (ORTEP drawing, 30% thermal ellipsoids). H atoms and guest water molecules are omitted for clarity. (b) A 2D sinusoidal-like layered framework built up via the bridges of Zn(II) ions and BT^{4-} ligands, viewed along the *a* axis (left) and *c* axis (right), respectively. (c) A 3D MOF built up via the bridges of 2D $[\text{Zn}_2\text{-BT}]$ layers (orange-red) and bpp ligands (green) viewed along the *a* axis (left) and *c* axis (middle). Right: the Zn...Zn distances via BT^{4-} ligand bridges. (d) Left: the sinusoidal-like water layer viewed along the *a* axis. Middle: the sinusoidal-like water layer viewed along the *c* axis. Right: the synergistic interactions between 2D water hydrogen-bonded layer and two $[\text{Zn}_2(\text{BT})]_n$ layers.

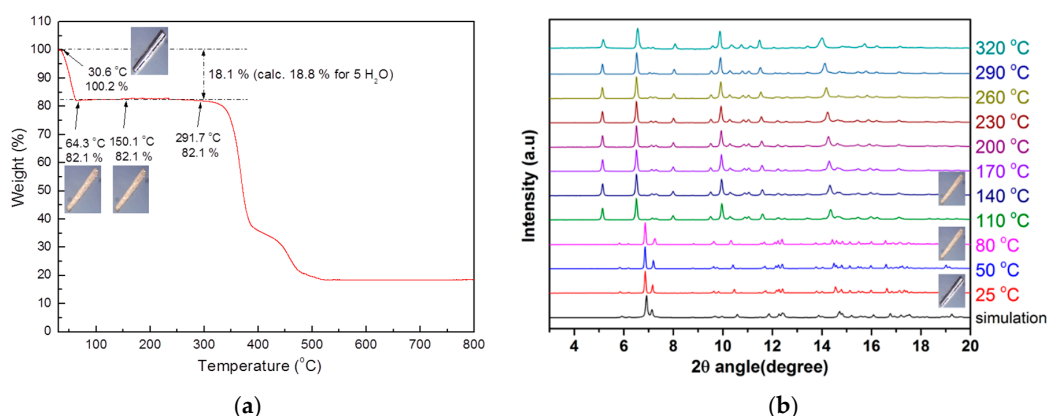


Figure 4. (a) Thermogravimetric (TG) analysis of **2** associated with morphological changes at selected temperatures. (b) Powder X-ray diffraction patterns at RT and selected temperatures and its simulation from single-crystal diffraction data associated with morphological changes at selected temperatures of **2**. The baselines for each temperature were shifted for clarity.

3.4. Water De-/Adsorption Behaviors of CPs **1** and **2** by Cyclic TG Analysis

In order to certify the reversibility of water de-/adsorption behaviors in **1** and **2** under water vapor, cyclic TG measurements were performed under de-/rehydration procedures by heating/cooling processes. Compound **1** showed a 20.0% weight decrease, corresponding to the losses of six coordinated H₂O molecules, 1.5 guest EtOH and 1.5 H₂O molecules, to obtain a dehydrated form of **1** after heating up to 120 °C (Figure 5a). When the dehydrated samples **1** were exposed to the water vapor and gradually cooled down to RT, the dehydrated samples showed a weight-increasing of 9.3%, approximately equal to 5.0 H₂O molecules, to form the rehydration ones. Such heating and cooling processes were repeated for five times (Figure 5a), showing almost equally weighted increasing/decreasing percentages in the range of 9.3~10.1%, to prove the stable reversibility of the water de-/rehydration behavior. On the contrary, compound **2** shows irreversible water de-/adsorption behavior during the cyclic TG measurements shown in Figure 5b, in which a 20.0% weight decrease was found in the first cycle, corresponding to the losses of five guest H₂O molecules, to obtain the dehydrated form **2** after heating up to 150 °C (Figure 5b). When the dehydrated samples **2** were exposed to the water vapor and cooled down to RT, the water molecules could not be re-adsorbed. The results described above show reversible water de-/adsorption behaviors between dehydrated and rehydrated forms, but **2** shows irreversible water de-/adsorption behavior. The poor water adsorption ability of dehydrated **2** may be attributed to the structural change of the dehydrated form, which may prevent the re-adsorption of water molecules via the synergistic hydrogen bonding interactions between water molecules and [Zn₂(BT)]_n layers.

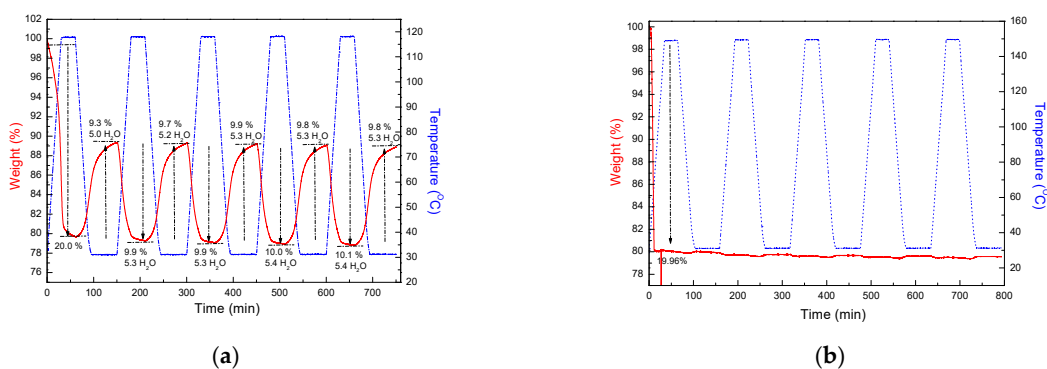


Figure 5. TG measurements of (a) **1** and (b) **2** during the cyclic de-/rehydration processes, which were repeated five times. Solid red line: the variation in weight loss with time; blue dash-dot line: the variation in temperature with time.

3.5. Water Sorption Studies of CP 1

According to cyclic TG analyses, compound **1** shows the reversible de-/adsorption behavior of approximately five water molecules. In order to explore the water adsorption ability of **1**, water vapor sorption isotherms of pre-treated dehydrated form **1** were measured at 298K. The isotherm curve (Figure 6) of dehydrated **1** shows a steady increase in adsorbed water vapor at $0 < \text{relative } P/P_0 < 0.89$, with maximum value of $210.7 \text{ cm}^3 \text{ g}^{-1}$ at relative P/P_0 equal to 0.89, approximately equal to 8.20 H_2O molecules, indicating six coordinated and two guest H_2O molecules in **1** being re-adsorbed. It is worth noting that the desorption curve did not trace the adsorption curve, exhibiting a significant hysteresis loop with a value of $148.5 \text{ cm}^3 \text{ g}^{-1}$, approximately equal to 5.8 H_2O molecules at lower relative P/P_0 equal to 0.22. The water ad-/desorption isotherms of dehydrated form **1** reveal that the vacant sites of Ni(II) ions provide the opportunity for bond re-formation with water molecules as the dehydrated samples being exposed to water vapor. Recently, MOFs with high porosity have been examined for their water capture properties and found to be highly promising materials [42–44]. However, water capture properties applied to 3D supramolecular architectures assembled via CPs or MOFs are seldom detected and only a few cases have been investigated [45–47]. The water sorption isotherm with large hysteresis loops found in **1** is interesting and may be exploited as a water harvesting material.

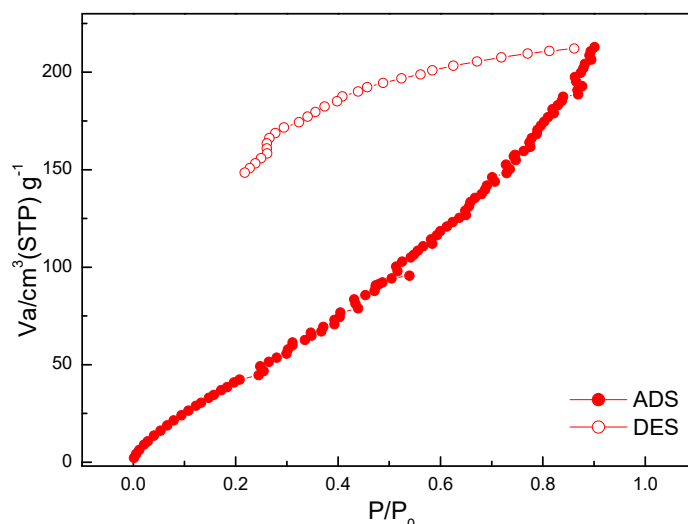


Figure 6. Water vapor ad-/desorption isotherms of dehydrated **1** at 298 K.

4. Conclusions

Two coordination polymeric frameworks, $\{[\text{Ni}_2(\text{bpp})_2(\text{BT})(\text{H}_2\text{O})_6] 1.5(\text{EtOH}) \cdot 1.5\text{H}_2\text{O}\}_n$ (**1**) and $[\text{Zn}(\text{bpp})(\text{BT})_{0.5}] \cdot 5\text{H}_2\text{O}$ (**2**), have been structurally investigated. In compound **1**, the 3D supramolecular architecture is built up via the assembly of 2D MOFs, which are constructed through the bridges of Ni(II) with 1,4-*bis*-monodentate *bpp* and BT^{4-} ligands. Compound **2** is a 3D MOF constructed through the bridges of Zn(II) with *bis*-monodentate *bpp* and 1,2,4,5-*tetrakis*-monodentate BT^{4-} ligands. Interestingly, the guest water molecules in **2** are assembled together to generate a 2D sinusoidal-like hydrogen-bonded water layer, which is built up by two water cluster units—one is a $(\text{H}_2\text{O})_6$ chair-like water ring and the other is a $(\text{H}_2\text{O})_{18}$ water ring—via the intermolecular $\text{O}-\text{H} \cdots \text{O}$ hydrogen bonding interactions. Notably, compound **1** exhibits interesting water hysteresis isotherms and undergoes reversible water de-/adsorption behavior between the dehydrated and rehydrated species during thermal re-/dehydration processes. Water capture uptake observed in **1** displayed significant hysteresis loops in water ad-/desorption isotherms, which may be developed for potential application as a water harvesting material.

Supplementary Materials: The following are available online at <http://www.mdpi.com/2073-4360/12/10/2222/s1>, Figure S1: (a) TG measurement of **1**, (b) PXRD patterns at RT and selected temperatures and their simulation from single-crystal diffraction data of **1**, Figure S2: (a) TG measurement of **2**, (b) PXRD patterns at RT and selected temperatures and their simulation from single-crystal diffraction data of **2**, Table S1: Bond lengths (Å) and angles (°) around Ni(II) ions in **1**, Table S2: Related parameters of hydrogen bonds in **1**, Table S3: Bond lengths (Å) and angles (°) around Zn(II) ion in **2**, Table S4: Related parameters of hydrogen bonds in **2**.

Author Contributions: C.-C.W. designed the experiments; W.-C.Y., Z.-L.H., W.-C.C., T.-W.C. and Y.-Y.T. completed the experiments, including synthesis, structural characterization, EA, IR, TG analysis, and water ad/desorption measurements; G.-H.L. contributed to the single-crystal X-ray data collection and structural analysis; B.-H.C. and Y.-C.C. contributed to the PXRD measurements by synchrotron radiation light source; C.-C.W. and Y.-C.C. wrote the paper. All authors have read and agreed to the published version of the manuscript.

Funding: This research received no external funding.

Acknowledgments: The authors wish to thank the Ministry of Science and Technology and Soochow University, Taiwan for the financial support.

Conflicts of Interest: The authors declare no conflict of interest.

References

1. Batten, S.R.; Champness, N.R.; Chen, X.-M.; Garcia-Martinez, J.; Kitagawa, S.; Öhrström, L.; O’Keeffe, M.; Suh, M.P.; Reedijk, J. Coordination polymers, metal–organic frameworks and the need for terminology guidelines. *CrystEngComm* **2012**, *14*, 3001–3004. [[CrossRef](#)]
2. Terminology of Metal-Organic Frameworks and Coordination Polymers. *Chem. Int.* **2013**, *35*, 1715–1724. [[CrossRef](#)]
3. Li, B.; Chrzanowski, M.; Zhang, Y.; Ma, S. Applications of metal-organic frameworks featuring multi-functional sites. *Coord. Chem. Rev.* **2016**, *307*, 106–129. [[CrossRef](#)]
4. Zhang, X.; Wang, W.; Hu, Z.; Wang, G.; Uvdal, K. Coordination polymers for energy transfer: Preparations, properties, sensing applications, and perspectives. *Coord. Chem. Rev.* **2015**, *284*, 206–235. [[CrossRef](#)]
5. Bradshaw, D.; Claridge, J.B.; Cussen, E.J.; Prior, T.J.; Rosseinsky, M.J. Design, Chirality, and Flexibility in Nanoporous Molecule-Based Materials. *Acc. Chem. Res.* **2015**, *38*, 273–282. [[CrossRef](#)]
6. Silva, P.; Vilela, S.M.F.; Tome, J.P.C.; Paz, F.A.A. Multifunctional metal–organic frameworks: From academia to industrial applications. *Chem. Soc. Rev.* **2015**, *44*, 6774–6803. [[CrossRef](#)]
7. Li, S.; Huo, F. Metal–organic framework composites: From fundamentals to applications. *Nanoscale* **2015**, *7*, 7482–7501. [[CrossRef](#)]
8. Janiak, C.; Vieth, J.K. MOFs, MILs and more: Concepts, properties and applications for porous coordination networks (PCNs). *New J. Chem.* **2010**, *34*, 2366. [[CrossRef](#)]
9. He, Y.; Li, B.; O’Keeffe, M.; Chen, B. Multifunctional metal–organic frameworks constructed from meta-benzenedicarboxylate units. *Chem. Soc. Rev.* **2014**, *43*, 5618–5656. [[CrossRef](#)]
10. Lin, Z.-J.; Lu, J.; Hong, M.; Cao, R. Metal–organic frameworks based on flexible ligands (FL-MOFs): Structures and applications. *Chem. Soc. Rev.* **2014**, *43*, 5867–5895. [[CrossRef](#)]
11. Jia, H.P.; Li, W.; Ju, Z.F.; Zhang, J. Co₅(μ₃-OH)₂(btec)₂(bpp)_n: A three-dimensional homometallic molecular metamagnet built from the mixed hydroxide/carboxylate-bridged ferromagnetic-like chains. *Dalton Trans.* **2007**, *33*, 3699–3704. [[CrossRef](#)] [[PubMed](#)]
12. Yang, E.-C.; Liu, Z.-Y.; Liu, T.-Y.; Li, L.-L.; Zhao, X.-J. Co-ligand-directed structural and magnetic diversities in an anisotropic CoII–triazolate system. *Dalton Trans.* **2011**, *40*, 8132. [[CrossRef](#)] [[PubMed](#)]
13. Zhao, L.M.; Li, H.H.; Wu, Y.; Zhang, S.Y.; Zhang, Z.J.; Shi, W.; Cheng, P.; Liao, D.Z.; Yan, S.P. Synthesis, crystal structures, and magnetic properties of Mn(II), Co(II), and Zn(II) coordination polymers containing 1,2,4,5-benzenetetracarboxylic acid and 4,4’-azobispyridine. *Eur. J. Inorg. Chem.* **2010**, *13*, 1983–1990. [[CrossRef](#)]
14. Fabelo, O.; Cañadillas-Delgado, L.; Pasaán, J.; Delgado, F.S.; Lloret, F.; Cano, J.; Julve, M.; Ruiz-Pérez, C. Study of the Influence of the Bridge on the Magnetic Coupling in Cobalt(II) Complexes. *Inorg. Chem.* **2009**, *48*, 11342–11351. [[CrossRef](#)] [[PubMed](#)]
15. Fabelo, O.; Pasán, J.; Cañadillas-Delgado, L.; Delgado, F.S.; Yuste, C.; Lloret, F.; Julve, M.; Ruiz-Pérez, C. Novel cobalt(II) coordination polymers based on 1,2,4,5-benzenetetracarboxylic acid and extended bis-monodentate ligands. *CrystEngComm* **2009**, *11*, 2169. [[CrossRef](#)]

16. Cheng, D.; Khan, M.A.; Houser, R.P. Novel Sandwich Coordination Polymers Composed of Cobalt(II), 1,2,4,5-Benzenetetracarboxylate Ligands, and Homopiperazonium Cations. *Cryst. Growth Des.* **2002**, *2*, 415–420. [[CrossRef](#)]
17. Sun, D.; Zhang, N.; Luo, G.; Xu, Q.-J.; Huang, R.-B.; Zheng, L.-S. Assembly of silver(I) coordination polymers incorporating pyromellitic acid and N-heterocyclic ligands. *Polyhedron* **2010**, *29*, 1842–1848. [[CrossRef](#)]
18. Ren, C.; Hou, L.; Liu, B.; Yang, G.; Wang, Y.-Y.; Shi, Q.-Z. Distinct structures of coordination polymers incorporating flexible triazole-based ligand: Topological diversities, crystal structures and property studies. *Dalton Trans.* **2011**, *40*, 793–804. [[CrossRef](#)]
19. Luo, G.; Wu, S.-H.; Zhao, Q.-H.; Li, D.; Xiao, Z.-J.; Dai, J.-C. Water helicate (H₂O)₅ hosted by a novel 2D CoII-coordination framework with left- and right-handed helical units. *Inorg. Chem. Commun.* **2012**, *20*, 290–294. [[CrossRef](#)]
20. Correa, C.C.; Diniz, R.; Janczak, J.; Yoshida, M.I.; De Oliveira, L.F.; Machado, F.C. High dimensional coordination polymers based on transition metals, 1,2,4,5-benzenetetracarboxylate anion and 1,3-bis(4-pyridyl)propane nitrogen ligand. *Polyhedron* **2010**, *29*, 3125–3131. [[CrossRef](#)]
21. Atria, A.M.; Corsini, G.; Garland, M.T.; Baggio, R. Poly[4,40-(propane-1,3-diyl)dipyridinium bis{tetraaquabis(μ-2,5-carboxybenzene-1,2,4-tricarboxylato)bis[μ-1,3-bis(4-pyridyl)propane]dicobalt(II)}pentahydrate]. *Acta Cryst.* **2011**, *67*, m367–m370.
22. Jeremias, F.; Khutia, A.; Janiak, C.; Henninger, S.K. MIL-100(Al, Fe) as water adsorbents for heat transformation purposes—A promising application. *J. Mater. Chem.* **2012**, *22*, 10148–10151. [[CrossRef](#)]
23. Cañadillas-Delgado, L.; Fabelo, O.; Ruiz-Pérez, C.; Delgado, F.S.; Julve, M.; Hernandez-Molina, M.; Laz, M.M.; Lorenzo-Luis, P.A. Zeolite-like Nanoporous Gadolinium Complexes Incorporating Alkaline Cations. *Cryst. Growth Des.* **2006**, *6*, 87–93. [[CrossRef](#)]
24. Majumder, A.; Gramlich, V.; Rosair, G.M.; Batten, S.R.; Masuda, J.D.; El Fallah, M.S.; Ribas, J.; Sutter, J.P.; Desplanches, C.; Mitra, S. Five New Cobalt(II) and Copper(II)-1,2,4,5-benzenetetracarboxylate Supramolecular Architectures: Syntheses, Structures, and Magnetic Properties. *Cryst. Growth Des.* **2006**, *6*, 2355–2368. [[CrossRef](#)]
25. Li, Y.; Hao, N.; Lu, Y.; Wang, E.; Kang, Z.; Hu, C. New Two-Dimensional Metal–Organic Networks Constructed from 1,2,4,5-Benzenetetracarboxylate and Chelate Ligands. *Inorg. Chem.* **2003**, *42*, 3119–3124. [[CrossRef](#)]
26. Fabelo, O.; Pasán, J.; Lloret, F.; Julve, M.; Ruiz-Pérez, C. 1,2,4,5-Benzenetetracarboxylate- and 2,2'-Bipyrimidine-Containing Cobalt(II) Coordination Polymers: Preparation, Crystal Structure, and Magnetic Properties. *Inorg. Chem.* **2008**, *47*, 3568–3576. [[CrossRef](#)]
27. Halim, R.A.; Bhatt, P.M.; Belmabkhout, Y.; Shkurenko, A.; Adil, K.; Barbour, L.J.; Eddaoudi, M. A Fine-Tuned Metal–Organic Framework for Autonomous Indoor Moisture Control. *J. Am. Chem. Soc.* **2017**, *139*, 10715–10722. [[CrossRef](#)]
28. Massoud, S.S.; Mautner, F.A.; Louka, F.R.; Demeshko, S.; Dechert, S.; Meyer, F. Diverse coordination of polynuclear copper(II) complexes constructed from benzene tetracarboxylates. *Inorg. Chim. Acta* **2011**, *370*, 435–443. [[CrossRef](#)]
29. Mautner, F.A.; Albering, J.H.; Vicente, R.; Andrepont, C.; Gautreaux, J.G.; Gallo, A.A.; Massoud, S.S. Synthesis, structure and magnetic investigations of polycarboxylate-copper(II) complexes. *Polyhedron* **2013**, *54*, 158–163. [[CrossRef](#)]
30. Li, X.-J.; Cao, R.; Bi, W.-H.; Wang, Y.-Q.; Wang, Y.; Li, X. Three interpenetrated frameworks constructed by long flexible N,N'-bipyridyl and dicarboxylate ligands. *Polyhedron* **2005**, *24*, 2955–2962. [[CrossRef](#)]
31. Lee, T.-W.; Lau, J.P.-K.; Wong, W.-T. Synthesis and characterization of coordination polymers of Zn(II) with 1,3-bis(4-pyridyl)propane and 4,4'-pyridine ligands. *Polyhedron* **2004**, *23*, 999–1002. [[CrossRef](#)]
32. Correa, C.C.; Diniz, R.; Chagas, L.H.; Rodrigues, B.L.; Yoshida, M.I.; Teles, W.M.; Machado, F.C.; De Oliveira, L.F.C. Transition metal complexes with squarate anion and the pyridyl-donor ligand 1,3-bis(4-pyridyl)propane (BPP): Synthesis, crystal structure and spectroscopic investigation. *Polyhedron* **2007**, *26*, 989–995. [[CrossRef](#)]
33. Plater, M.J.; Foreman, M.R.S.; Gelbrich, T.; Hursthouse, M.B. One-dimensional structures of nickel(II) and cobalt(II) coordination complexes {[ML₂(H₂O)₂]·L·H₂O·(ClO₄)₂} (M = Co or Ni; L = 1,3-bis(4-pyridyl)propane) *Inorg. Chim. Acta* **2001**, *318*, 171–174.

34. Maw-Cherng, S.; Chan, Z.K.; Chen, J.D.; Wang, J.C.; Hung, C.H. Syntheses and structures of three new coordination polymers generated from the flexible 1,3-bis(4-pyridyl)propane ligand and zinc salts. *Polyhedron* **2006**, *25*, 2325–2332.
35. Carlucci, L.; Ciani, G.; Proserpio, D.M.; Rizzato, S. New polymeric networks from the self-assembly of silver(i) salts and the flexible ligand 1,3-bis(4-pyridyl)propane (bpp). A systematic investigation of the effects of the counterions and a survey of the coordination polymers based on bpp. *CrystEngComm* **2002**, *4*, 121–129. [[CrossRef](#)]
36. Gao, E.-Q.; Xu, Y.-X.; Cheng, A.-L.; He, M.-Y.; Yan, C.-H. Copper(II) and cobalt(II) coordination polymers with azido ions and 1,3-bis(4'-pyridyl)propane. *Inorg. Chem. Commun.* **2006**, *9*, 212–215. [[CrossRef](#)]
37. *SMART V 4.043 Software for CCD Detector System*; Siemens Analytical Instruments Division: Madison, WI, USA, 1995.
38. *SAINT V 4.035 Software for CCD Detector System*; Siemens Analytical Instruments Division: Madison, WI, USA, 1995.
39. Sheldrick, G.M. *Program for the Refinement of Crystal Structures*; University of Göttingen: Göttingen, Germany, 1993.
40. *SHELXTL 5.03 (PC-Version), Program Library for Structure Solution and Molecular Graphics*; Siemens Analytical Instruments Division: Madison, WI, USA, 1995.
41. Toby, B.H.; Von Dreele, R.B. GSAS-II: The genesis of a modern open-source all purpose crystallography software package. *J. Appl. Crystallogr.* **2013**, *46*, 544–549. [[CrossRef](#)]
42. Yilmaz, G.; Peh, S.B.; Zhao, D.; Ho, G.W. Atomic- and Molecular-Level Design of Functional Metal–Organic Frameworks (MOFs) and Derivatives for Energy and Environmental Applications. *Adv. Sci.* **2019**, *6*. [[CrossRef](#)]
43. Rieth, A.J.; Wright, A.M.; Skorupskii, G.; Mancuso, J.L.; Hendon, C.H.; Dincă, M. Diverse π – π stacking motifs modulate electrical conductivity in tetrathiafulvalene-based metal–organic frameworks. *J. Am. Chem. Soc.* **2019**, *141*, 13858–13866. [[CrossRef](#)]
44. Furukawa, H.; Gándara, F.; Zhang, Y.-B.; Jiang, J.; Queen, W.L.; Hudson, M.R.; Yaghi, O.M. Water Adsorption in Porous Metal–Organic Frameworks and Related Materials. *J. Am. Chem. Soc.* **2014**, *136*, 4369–4381. [[CrossRef](#)]
45. Wang, C.C.; Ke, S.Y.; Chen, K.T.; Sun, N.K.; Liu, W.F.; Ho, M.L.; Lu, B.J.; Hsieh, Y.T.; Lee, G.H.; Huang, S.Y.; et al. Sponge-Like Water De-/Ad-Sorption versus Solid-State Structural Transformation and Colour-Changing Behavior of an Entangled 3D Composite Supramolecular Architecture, $[\text{Ni}_4(\text{dpe})_4(\text{btc})_2(\text{Hbtc})(\text{H}_2\text{O})_9] \cdot 3\text{H}_2\text{O}$. *Polymers* **2018**, *10*, 1014. [[CrossRef](#)] [[PubMed](#)]
46. Ke, S.Y.; Chang, Y.F.; Wang, H.Y.; Yang, C.C.; Ni, C.W.; Lin, G.Y.; Chen, T.T.; Ho, M.L.; Lee, G.H.; Chuang, Y.C.; et al. Self-Assembly of Four Coordination Polymers (CPs) in A 3D Entangled Architecture Showing Reversible Dynamic Solid-State Structural Transformation and Color-Changing Behaviour by Thermal De-/Re-hydration. *Cryst. Growth Des.* **2014**, *14*, 4011–4018. [[CrossRef](#)]
47. Fukushima, T.; Horike, S.; Inubushi, Y.; Nakagawa, K.; Kubota, Y.; Takata, M.; Kitagawa, S. Solid Solutions of Soft Porous Coordination Polymers: Fine-Tuning of Gas Adsorption Properties. *Angw. Chem. Int. Ed.* **2010**, *49*, 4820–4824. [[CrossRef](#)] [[PubMed](#)]

